Backaction suppression in levitated optomechanics using reflective boundaries

Rafał Gajewski and James Bateman*
Department of Physics, Faculty of Science and Engineering, Swansea University, Swansea SA2 8PP, Wales, United Kingdom

(Received 10 May 2024; accepted 3 March 2025; published 11 April 2025)

We show theoretically that the noise due to laser induced backaction acting on a small nanosphere levitated in a standing-wave trap can be considerably reduced by utilizing a suitable reflective boundary. We examine the spherical mirror geometry as a case study of this backaction suppression effect, discussing the theoretical and experimental constraints. We study the effects of laser recoil directly, by analyzing optical force fluctuations acting on a dipolar particle trapped at the center of a spherical mirror. We also compute the corresponding measurement imprecision in an interferometric, shot-noise-limited position measurement, using the formalism of Fisher information flow. Our results show that the standing-wave trapping field is necessary for backaction suppression in three dimensions, and they satisfy the Heisenberg limit of detection.

DOI: 10.1103/PhysRevResearch.7.023041

I. INTRODUCTION

In recent years, experiments which utilize nanosized particles trapped at the focus of a laser beam emerged as a promising experimental platform for detecting ultrasmall forces [1,2], gravitational waves [3], searching for dark matter [4], and potentially probing quantum behaviors of large masses in wide and untested parameter regimes [5]. These levitated optomechanical systems constitute high quality mechanical oscillators, the position of which is probed by phase-sensitive measurement of the light scattered by the particle. The interferometric position readout and extreme isolation from thermal dissipation [6], reached due to the lack of physical contact, enabled levitated optomechanical systems to cool the particle motion to the ground state [7–9], with recent experiments showing prospects for quantum-enhanced sensing below the shot-noise level [10].

However, in a continuous measurement by the laser, fluctuations of the electromagnetic field introduce random perturbations to the motion of the mass known as measurement backaction [11–14]. This backaction noise is linked to the minimum achievable imprecision in the position measurement by the Heisenberg limit of detection [13,15], which keeps the product of the two quantities fixed. Although cooling of the particle to its motional ground state has been demonstrated [7–9], the coherence times of the prepared motional states are limited by excessive recoil heating imposed by the optical measurement process. This limits access to the envisioned applications [6] and therefore finding ways to mitigate the effects of backaction is of vital importance.

The degree to which the backaction process can be controlled in levitated optomechanics without turning off the trapping light has not yet been fully explored. Recently, a backaction suppression method has been proposed based on illumination by squeezed light [16], enabling control over the information encoded in the radiation scattered by the particle. A different method relies on trapping hexagonal plates instead of spheres [3,17], because a different geometry of the trapped object alters its radiation pattern, thereby confining the solid angle in which backaction noise can act.

Backaction noise in levitated optomechanics can be understood as a result of interference of the laser field with the local vacuum field fluctuations [12,18–20]. In general, the vacuum fluctuations are a function of the environment, depending on its material properties and geometry [21,22]. It is known that surfaces can lead to backaction different from what would be expected in free space [19]. In this paper, we investigate an experimental scheme to suppress backaction by trapping the particle at the center of a spherical mirror. We show that a spherical geometry in conjunction with a standing-wave optical trapping potential can lead to a substantial reduction in mechanical noise, limited mainly by the mirror reflectivity.

Previous QED analysis of the spherical mirror geometry found that the local density of optical states is strongly modified at the center [23], which allows for full suppression of spontaneous emission from an atom. In the context of levitated optomechanics, optimal position measurement of a particle trapped at the center of a spherical mirror was recently analyzed [24,25] and the authors show that this can be used to realize an ideal reference field for self-homodyne detection which is theoretically able to reach the Heisenberg limit of detection by observation from only half of the solid angle.

A similar setup was also recently proposed for the purpose of backaction suppression [26]. While our findings do not contradict the general protocol presented in this recent paper, we find that suppression of scattered power *does not* correspond to the suppression of backaction. Instead, we find that the linear position readout becomes inaccessible in an

*Contact author: j.e.bateman@swansea.ac.uk

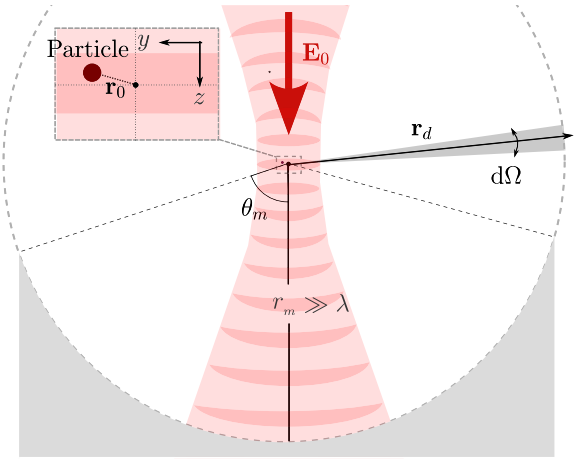

FIG. 1. Spherical mirror trapping configuration. A laser beam polarized out of the page is focused close to the center of the spherical mirror, such that the beam retroreflects from the mirror surface and generates a standing-wave trap. A particle is trapped at the central maximum with displacement from the center $|\mathbf{r}_0| \ll \lambda$.

interferometric measurement of the far-field scatter when the scattered power is *maximally enhanced* by the spherical mirror. Our results suggest that the scheme of constraining backaction noise presented in Ref. [26] could be successfully applied with a small adjustment of the spherical mirror radius. We also find that full backaction suppression effect in three dimensions is possible when the spherical mirror covers half of the solid angle and the light probing the position of the particle corresponds to a maximum of an intensity standing wave. We show that our results satisfy the Heisenberg limit of detection, and therefore constitute a tradeoff between measurement imprecision and backaction without altering the illuminating laser power. This paper has general implications for recoil noise reduction in a structured environment, offers a feasible experimental implementation, and may aid in the search for other useful configurations.

II. PROBLEM STATEMENT

We consider the setup shown in Fig. 1 as a case study. In this setup, the beam is incident upon the mirror surface and forms a standing-wave trap. We assume that the beam parameters are selected such that the beam is retroreflected and an intensity maximum appears at the mirror center (see Appendix C) which we also take to be the origin of the coordinate system. The particle is trapped at the intensity maximum appearing at the center of a spherical mirror, and is located at $\mathbf{r}_0$ (with $|\mathbf{r}_0| \ll \lambda$) which corresponds to the displacement due to the motion about the trap center. The particle is modeled as a point electric dipole [22] (radius $r_p \ll \lambda$) with isotropic polarizability α acted on by a stochastic force $\delta\mathbf{F}$. We assume that we can ignore the contribution of residual gas and that the force fluctuations are dominated by the contribution from laser recoil. Throughout this paper, we work in the quasistatic limit, ignoring any effects the motion has on the imprecision-backaction characteristics. Assuming that the mirror is not too large, this is permissible since the particle motion is significantly slower than time delay of the mirror-particle round trip.

We assume that the beam is weakly focused and that the central maximum is sufficiently close to the beam waist such that the standing-wave field resembles a field of two counter-propagating plane waves:

$$\mathbf{E}_0(\mathbf{r}, t) = \mathrm{Re}[E_0 \cos(Akz) e^{-i\omega_0 t}]\hat{\mathbf{x}}. \tag{1}$$

In Eq. (1), $k = \omega_0/c = 2\pi/\lambda$ is the free-space wave number of the laser beam and the Gouy factor A increases the effective wavelength of the field, depending on the degree of focusing [15]. We note that the standing wave as shown in Fig. 1 depends on the mirror radius. We address the question of maintaining an intensity maximum (and therefore the equilibrium trapping position) at the center of the mirror in Appendix C.

In the next section, we compute measurement backaction by employing a stochastic electrodynamics description of the local field fluctuations [18,20,27–29] and computing the spectral noise density of the recoil force in a standing wave with an intensity maximum at the mirror center, *independent of how the standing wave was formed*. The results of Sec. III and Appendix C show that the condition on the mirror radius required to keep an intensity maximum of a standing wave at the center coincides with the condition corresponding to full suppression of backaction noise. Therefore, the setup shown in Fig. 1 shows how our results can be applied in an experiment to demonstrate suppression of backaction in three dimensions.

III. MEASUREMENT BACKACTION

In this section we quantify the measurement backaction by computing the spectral density of the optical force fluctuations at the mechanical frequency of the trapped particle. In previous studies, recoil was inferred from the radiation pressure that the dipole emission would exert in the far field [15,24,26]. However, when reflective boundaries are present, it is unclear whether this approach is valid, since the direction of recoil depends on how the scattered radiation maps to its reflection in the far field. Here, we instead compute the optical force directly at the location of the particle.

The particle interacts with the laser field and a fluctuating background field:

$$\mathbf{E}(\mathbf{r}_0, t) = \mathbf{E}_0(\mathbf{r}_0, t) + \delta\mathbf{E}(\mathbf{r}_0, t). \tag{2}$$

In Eq. (2), $\delta\mathbf{E}$ represent zero-point or thermal field fluctuations that are modeled as a statistically stationary process with zero average [20], and $\mathbf{E}_0$ is the trapping laser field. In general, the particle also interacts with reflections of its own scatter, which lead to an infinite series of additional terms in Eq. (2) scaling in powers of $k^3\alpha$. Since $k^3\alpha \sim (r_p/\lambda)^3 \ll 1$ this series converges quickly, and since we are interested in computing the dominating contribution to backaction, we truncate at zeroth order in α. Treating the particle as a point electric dipole located at $\mathbf{r}_0$, the field in Eq. (2) induces a dipole moment $\mathbf{p}$. In this dipole approximation, the particle experiences an optical force given by [22]

$$\mathbf{F} = \sum_i p_i \nabla E_i + \frac{d}{dt}(\mathbf{p} \times \mathbf{B}) \tag{3}$$

where $i = x, y, z$. Since we are only interested in computing the contribution of laser recoil, we ignore the intrinsic fluctuations of the dipole moment. In the frequency domain in the limit $\omega \ll \omega_0$, the force is well approximated by the first term in Eq. (3):

$$\tilde{\mathbf{F}}(\mathbf{r}_0, \omega) = \sum_i (\tilde{p}_i * \nabla \tilde{E}_i)(\mathbf{r}_0, \omega) \approx \tilde{\mathbf{F}}_0(\mathbf{r}_0, \omega) + \delta\tilde{\mathbf{F}}(\mathbf{r}_0, \omega) \tag{4}$$

where the quantities with a tilde denote the respective Fourier transforms and the asterisk symbol denotes a convolution[1] in frequency. In the second line of Eq. (4) we chose $\tilde{\mathbf{F}}$ to represent the deterministic force and $\delta\tilde{\mathbf{F}}$ to represent force fluctuations, approximated with terms containing fluctuations in the fields up to linear order:

$$\delta\tilde{\mathbf{F}}(\mathbf{r}_0, \omega) = (\alpha\tilde{E}_0 * \nabla\delta\tilde{E})(\mathbf{r}_0, \omega) + (\alpha\delta\tilde{E} * \nabla\tilde{E}_0)(\mathbf{r}_0, \omega), \tag{5}$$

where we used $\tilde{\mathbf{p}} = \alpha\tilde{\mathbf{E}}$ and have assumed that $\mathbf{E}_0$ is $\hat{\mathbf{x}}$ polarized, which allows us to drop the subscript x from the field components δE_x and E_{0x} for clarity. Assuming that $\delta\tilde{\mathbf{F}}$ is a stationary stochastic process with zero ensemble average, we find the corresponding spectral density of the force fluctuations using the expression [30]

$$S^F_{ii}(\omega) = \int_{\mathbb{R}} \langle \delta\tilde{F}^*_i(\mathbf{r}_0, \omega)\delta\tilde{F}_i(\mathbf{r}'_0, \omega')\rangle \, \mathrm{d}\omega' \Big|_{\mathbf{r}_0=\mathbf{r}'_0}, \tag{6}$$

where the angled brackets denote an ensemble average. We can evaluate the field correlations arising in Eq. (6) by applying the fluctuation-dissipation theorem for the field fluctuations given in Eq. (A5). Upon substitution of Eqs. (5) and (A5) into Eq. (6), we find that for a monochromatic driving field of the form $\mathbf{E}(\mathbf{r}, t) = \mathrm{Re}[\tilde{E}(\mathbf{r})e^{-i\omega_0 t}]\hat{\mathbf{x}}$, the spectral density of force fluctuations in the limit $\hbar\omega_0 \gg k_B T$ can be approximated as [31]

$$\begin{aligned} S^F_{ii}(\omega) = \frac{\hbar\omega_0^2}{4\pi c^2\epsilon_0}\alpha^2\{&\tilde{E}^*_0(\mathbf{r}_0)\tilde{E}_0(\mathbf{r}'_0)\partial_i\partial'_i\mathrm{Im}[G_{xx}(\mathbf{r}_0, \mathbf{r}'_0, \omega_0)] \\ &+ \partial_i\tilde{E}^*_0(\mathbf{r}_0)\partial'_i\tilde{E}_0(\mathbf{r}'_0)\mathrm{Im}[G_{xx}(\mathbf{r}_0, \mathbf{r}'_0, \omega_0)] \\ &+ \tilde{E}^*_0(\mathbf{r}_0)\partial'_i\tilde{E}_0(\mathbf{r}'_0)\partial_i\mathrm{Im}[G_{xx}(\mathbf{r}_0, \mathbf{r}'_0, \omega_0)] \\ &+ \tilde{E}_0(\mathbf{r}'_0)\partial_i\tilde{E}^*_0(\mathbf{r}_0)\partial'_i\mathrm{Im}[G_{xx}(\mathbf{r}_0, \mathbf{r}'_0, \omega_0)]\}_{\mathbf{r}_0=\mathbf{r}'_0} \end{aligned} \tag{7}$$

where we introduced the dyadic Green's function of the system (see Appendix A) and defined the free-space scattered power $P_0 = E_0^2\alpha^2k^4c/(12\pi\epsilon_0)$ and the partial derivatives $\partial_i \equiv \partial/\partial x_i$ and $\partial'_i \equiv \partial/\partial x'_i$ with respect to the first and second argument of the Green's function respectively. As long as the aforementioned approximations apply, Eq. (7) represents the dominating term of backaction noise experienced by the particle in a driving laser field polarized along $\hat{\mathbf{x}}$ and an arbitrary environment described by G_{xx}. Physically, the first and second terms in Eq. (7) correspond to noise in the gradient force and the scattering force respectively, while the remaining terms represent the force correlations. For the case of a standing wave in Eq. (1), at an intensity maximum, where the particle is trapped, the expression in Eq. (7) can be further approximated as

$$S^F_{ii}(\omega) \approx \frac{3\hbar P_0}{k^2 c}\partial_i\partial'_i\mathrm{Im}[G_{xx}(\mathbf{r}_0, \mathbf{r}'_0, \omega_0)]_{\mathbf{r}_0=\mathbf{r}'_0} \tag{8}$$

leaving only the noise in the gradient force. In general, the gradient of the driving field in Eq. (7) gives rise to additional terms in the force spectral density. However, in the case of a particle trapped about an intensity maximum of a standing wave, with the assumption that $|\mathbf{r}_0| \ll \lambda$, the noise in the scattering force and the force correlations do not contribute up to second order in particle position [32]. In the case of a particle trapped at the focus of a single focused beam in free space, we recover the expressions for optimal position detection found in Ref. [15] including the terms which contain the factor A corresponding to the gradient of the focused field. The remaining term in Eq. (8) corresponds to the spectral density of the field gradient fluctuations. Within our approximations, our expression agrees with the expression for the decoherence rate due to laser recoil [19] for a model of a particle trapped in front of a flat plane, in the framework of macroscopic QED [33,34]. In that context, the dominant contribution to the noise arises from the driven-Casimir–Polder interaction term in the Hamiltonian of the trapped particle dynamics. This term is a result of interference of the classical driving field with medium-assisted vacuum fields. In addition, we note that for a standing wave under our approximations, the orientation of the beam axis does not enter the expression. Therefore, more generally the same expression holds for a standing wave rotated about the polarization vector.

We find the effect of the mirror on the force spectral density by substituting into Eq. (8) the Green's function which characterizes the spherical mirror geometry, as discussed in Appendix A. The resulting total Green's function is given by Eq. (A7), which upon substitution into Eq. (8) yields

$$S^F_{ii}(\omega) = \frac{\hbar k P_0}{2\pi c}\left[\frac{1}{5}(2 - \delta_{ix}\delta_{xi}) - 2\cos(2kr_m)\int_{(\mathrm{a})} \mathrm{d}S_{ii}\right] \tag{9}$$

which represents the modified backaction noise of a particle trapped in a standing wave at the center of a spherical mirror. In Eq. (9) δ_{xi} and δ_{ix} represent the Kronecker delta and we introduced

$$\mathrm{d}S_{ii} = (\hat{r}_i)^2\rho_x(\theta, \phi)\,\mathrm{d}\Omega \tag{10}$$

with the radiation pattern of an $\hat{\mathbf{x}}$ oriented dipole:

$$\rho_x(\theta, \phi) = \frac{3}{8\pi}[1 - (\hat{\mathbf{x}} \cdot \hat{\mathbf{r}})^2] \tag{11}$$

where the radial unit vector is given by $\hat{\mathbf{r}} = (\sin\theta\cos\phi, \sin\theta\sin\phi, \cos\theta)$. The first term in Eq. (9) represents the free-space backaction in a standing wave, while the second represents the contribution of the mirror. The integration in the second term runs over the mirror surface as depicted in Fig. 3. For a full hemispherical mirror, the result in Eq. (9) simplifies to

$$S^F_{ii}(\omega) = \frac{2}{5}\frac{\hbar k P_0}{2\pi c}\sin^2(kr_m)(2 - \delta_{ix}\delta_{xi}) \tag{12}$$

[1]The convolution is defined as $\{\tilde{a} * \tilde{b}\}(\mathbf{r}_0, \omega) = \int_{\mathbb{R}} \tilde{a}(\mathbf{r}_0, \Omega)\tilde{b}(\mathbf{r}_0, \omega - \Omega)\mathrm{d}\Omega$ and element-wise when one argument is a vector or tensor.

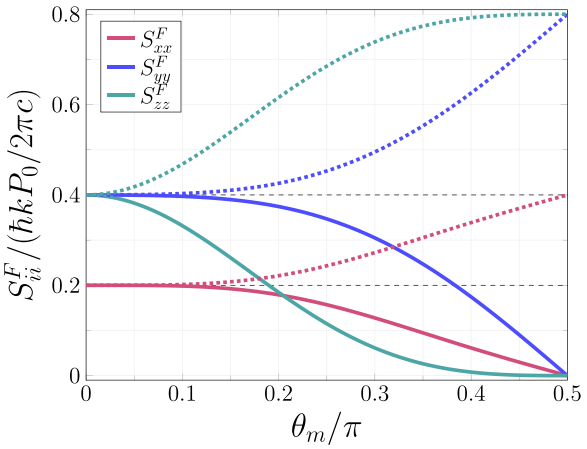

FIG. 2. Backaction $S^F_{ii}(\omega)$ against spherical mirror spanning angle found by solving Eq. (9). Filled lines indicate backaction for $kr_m = n\pi$ while dotted lines indicate backaction for $kr_m = n\pi \pm \pi/2$. Dashed lines indicate free-space levels in a standing wave, which in our model corresponds to $\theta_m = 0$.

which shows that for $kr_m = n\pi$ with integer n the dominating contribution to backaction noise vanishes. This *backaction suppression condition* coincides with the condition on the mirror radius needed for trapping at the mirror center (see Appendix C) and is also the condition giving maximum enhancement of scattered power (see Appendix B). This is in contrast to recent findings for the spherical mirror system [26] in which the authors assume that the suppression of scattered radiation leads to the suppression of backaction, based on previous backaction calculations in the literature for a particle scattering in free space [15]. Our result suggests that to effectively implement the protocol of Ref. [26], which inhibits the backaction in the control region, requires tuning the relationship between the mirror radius and the wavelength

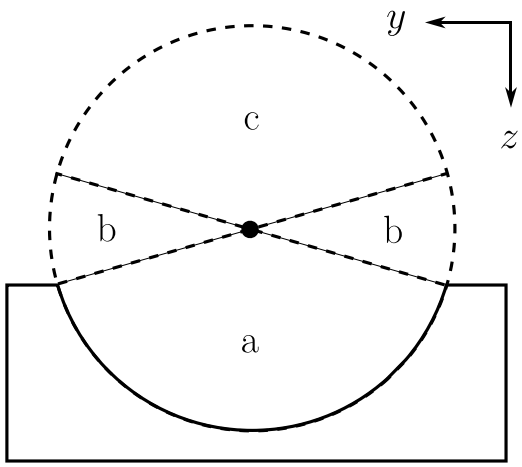

FIG. 3. Diagram denoting different measurement domains. For a spherical mirror that is perfectly reflecting, no field gets transmitted and dipole emission is not accessible for measurement within panel (a). Because dipole scatter is retroreflected by the mirror surface, the mirror only affects the detected emission in panel (c), while panel (b) corresponds to free-space dipole emission. (b) and (c) The dipole emission fields are given by Eqs. (16) and (17) respectively.

to yield maximum enhancement of scattered radiation, instead of radiation suppression. In addition, our result shows that the full backaction suppression in three dimensions is enabled in a standing-wave trapping field, in which case Eq. (8) is valid and the phase gradient of the driving field does not lead to additional contributions to backaction [32]. While the spherical geometry facilitates suppression of field gradient fluctuations, a standing-wave trapping configuration is necessary to suppress residual field amplitude fluctuations. In the next section, we consider the minimum measurement imprecision achievable in an interferometric measurement of the particle's position.

In Fig. 2 we also show how the backaction noise in (9) varies with the mirror polar angle θ_m, and find that the rate at which backaction decreases with $kr_m = n\pi$ is faster for S^F_{zz} than for S^F_{xx} and S^F_{yy}. This can be understood by considering the distribution of position information radiated into the far field, which we introduce in the next section.

IV. MEASUREMENT IMPRECISION

In recent studies involving the spherical mirror geometry [24,26], the achievable measurement imprecision is analyzed in the context of a self-homodyne measurement, that is, a measurement in which the reflection of the particle emission acts as the reference field. This approach does not reveal the imprecision which is generally achievable in the spherical mirror geometry, when a strong, mode-matched reference field is available [15]. In this paper, we formally quantify minimum measurement imprecision in the far-field shot-noise-limited detection of particle position using the recently developed formalism of Fisher information (FI) flow [35], which places a lower bound on the variance in the measured quantity. Specifically, the formalism introduces a local quantity of Fisher information flow, akin to the Poynting vector which describes the flow of electromagnetic energy. In the time average, the reciprocal of this quantity then places a bound on the average rate at which the variance of a variable can be reduced in a given bandwidth of shot-noise-limited measurement. The treatment is equivalent to treating the problem of an ideal interference experiment with a strong, mode-matching reference field [15,35]. The formalism reproduces the same results but avoids introducing an ideal reference field [15], by instead considering small perturbations to particle position via spatial derivatives. In a 1-Hz bandwidth we have

$$\mathrm{Var}(x_i) \geqslant \left(2\pi \int \mathbf{S}^{\mathrm{FI}}_{ii} \cdot \hat{\mathbf{r}}\, \mathrm{d}A\right)^{-1} 2\pi\,[\mathrm{Hz}] \tag{13}$$

where

$$\mathbf{S}^{\mathrm{FI}}_{ii} = \frac{2}{\hbar\omega_0}\mathrm{Re}[\partial_i \mathbf{E}_s \times \partial_i \mathbf{H}^*_s] \tag{14}$$

defines the time-averaged FI flux for the far fields $\mathbf{E}_s$ and $\mathbf{H}_s$ with $\partial_i \equiv \partial/\partial x_i$, and the quantity in parentheses in Eq. (13) corresponds to the flat spectral density of minimum imprecision noise,

$$S^{\mathrm{imp}}_{ii} = \left(2\pi \int \mathbf{S}^{\mathrm{FI}}_{ii} \cdot \hat{\mathbf{r}}\, \mathrm{d}A\right)^{-1}, \tag{15}$$

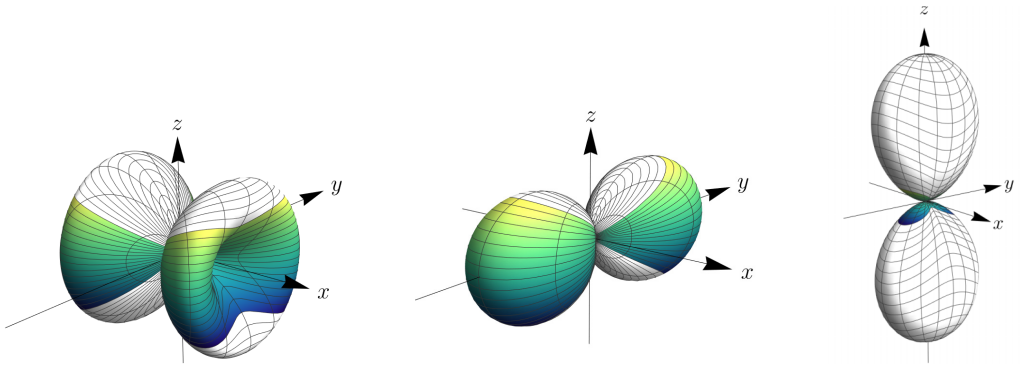

$\mathcal{I}_x(\theta,\phi)$ $\mathcal{I}_y(\theta,\phi)$ $\mathcal{I}_z(\theta,\phi)$

FIG. 4. Angular spread of position information, here defined as the integrand of Eq. (18) normalized to the free-space imprecision in a standing wave $S_{ii}^{\rm imp}(\theta_m = 0)$. The mirror is perfectly reflecting, has its axis of symmetry along $\hat{\mathbf{z}}$ as in Fig. 1, and was chosen to have $\theta_m = \pi/3$. The white region corresponds to domains (a) and (c) of Fig. 3. The information in the white region of the top half space (a) is never accessible because this portion of the solid angle is covered by the mirror, while information in panel (c) is rendered inaccessible by our suppression scheme. At $kr_m = n\pi$ the position information is inaccessible in the white region of both half spaces (a) and (b). The colored region corresponds to free-space information in a standing wave.

in the measurement of x_i. To obtain an optimal estimate of the particle's position for a general mirror spanning angle, we need to find $\mathbf{S}_{ii}^{\rm FI}$ in each angular domain at some large distance r_d over the angular element $\mathrm{d}A = r_d^2\,\mathrm{d}\Omega$, as depicted in Fig. 3. In domain (b) of Fig. 3, the dipole emission is unaffected by the mirror and hence the electric field is equal to the free-space dipole emission field driven by the field in Eq. (1):

$$\mathbf{E}_s^{(b)}(\mathbf{r}_d, \mathbf{r}_0) = \mathbf{E}_s(\mathbf{r}_d)\cos(Akz_0)e^{-ik\hat{\mathbf{r}}\cdot\mathbf{r}_0} \tag{16}$$

where we expanded $r' = |\mathbf{r}_d - \mathbf{r}_0| \approx r_d - \hat{\mathbf{r}}\cdot\mathbf{r}_0$ and where $\hat{\mathbf{r}} = (\sin\theta\cos\phi, \sin\theta\sin\phi, \cos\theta)$. The fields in Eq. (16) $\mathbf{E}_s^{(b)}(\mathbf{r}_d, \mathbf{r}_0)$ and $\mathbf{E}_s(\mathbf{r}_d)$ represent the complex field amplitudes in domain (b) of Fig. 3 from a dipole oriented along $\hat{\mathbf{x}}$ and located at position $\mathbf{r}_0$ and the origin respectively [see also Eq. (A4)]. In domain (c) of Fig. 3, the fields are a sum of the free-space dipole emission and its reflection from the spherical mirror. For a perfectly reflecting mirror and small displacement of the dipole from the mirror center, we find the field in domain (c) of Fig. 3 to be [36]

$$\mathbf{E}_s^{(c)}(\mathbf{r}_d) = \mathbf{E}_s(\mathbf{r}_d)e^{ikr_m}\cos(Akz_0)\cos(k[r_m + \hat{\mathbf{r}}\cdot\mathbf{r}_0]). \tag{17}$$

Note that in the field in Eq. (17) the free-space dipole emission and its reflection are in-phase. This is because the reflected field undergoes a change of sign upon propagating through the focus from the mirror surface to domain (c) of Fig. 3, akin to the Gouy shift of a focused Gaussian beam [37].

Substituting these fields into Eq. (15) and evaluating the derivatives about the mirror center yields the final result for a general spanning angle of the mirror:

$$S_{ii}^{\rm imp} = \left(\frac{8\pi kP_0}{\hbar c}\left[\int_{\rm (b)} \mathrm{d}S_{ii} + 4\sin(kr_m)^2\int_{\rm (c)} \mathrm{d}S_{ii}\right]\right)^{-1} \tag{18}$$

where $\mathrm{d}S_{ii}$ is given by Eq. (10). In the absence of the mirror [vanishing of domain (c) in Fig. 3], the expression in Eq. (18) recovers the expressions for free space from Ref. [15] with the exception of the term proportional to the factor A along the beam propagation direction. This is because in a standing-wave field, the field gradient does not carry linear position information. For a full hemisphere, the result in Eq. (18) reduces to

$$S_{ii}^{\rm imp} = \frac{5}{8}\frac{\hbar c}{\pi k}\frac{1}{P_0}\sin(kr_m)^{-2}(1 + \delta_{ix}\delta_{xi}). \tag{19}$$

Equation (19) diverges at the backaction suppression condition found in the previous section, suggesting that the emission from the particle available for measurement contains no first-order position information. Indeed, when $kr_m = n\pi$ the total emission field in the available solid angle,

$$\mathbf{E}_s^{(c)}(\mathbf{r}_d, \mathbf{r}_0) \approx 2\mathbf{E}_s(\mathbf{r}_d), \tag{20}$$

is independent of the source position to first order; the free-space dipole emission is in-phase with the emission from the image dipole [38], making it impossible to distinguish between them to first order.

Let us also remark on the distribution of available position information in the context of the angular information patterns which are employed in the literature [15,16]. In Fig. 4 we show the distribution of radiated position information for a spherical mirror with an illustrative spanning angle of $\theta_m = \pi/3$. The shapes of the corresponding information patterns are unchanged from free-space patterns in a standing wave, but the amount of information changes discontinuously between angular domains depicted in Fig. 4. Note that the distribution of the $\mathcal{I}_z(\theta,\phi)$ information differs from that given in Ref. [15]; in a standing-wave field, the information about the position along $\hat{\mathbf{z}}$ is radiated symmetrically about the xy plane. For a perfectly reflecting mirror at $kr_m = n\pi$, the position information is inaccessible in domains (a) and (c) of Fig. 3. In addition, Fig. 4 shows that at $\theta_m = \pi/3$ a significantly larger portion of the $\mathcal{I}_z$ solid angle is affected by the mirror compared with $\mathcal{I}_x$ and $\mathcal{I}_y$. The spherical mirror with its axis of symmetry aligned along the axis of the standing wave is particularly well suited for suppression of position information along the axis. This is also visible in the corresponding plot of backaction noise against θ_m in Fig. 2, which shows that the noise along $\hat{\mathbf{z}}$ changes more rapidly with θ_m than along $\hat{\mathbf{x}}$ and $\hat{\mathbf{y}}$.

V. DISCUSSION

We find that the product of the imprecision in Eq. (19) and the backaction in Eq. (12) satisfies the Heisenberg limit of detection [13,15],

$$S_{ii}^{F} S_{ii}^{\mathrm{imp}} = \left(\frac{\hbar}{2\pi}\right)^{2}, \tag{21}$$

for any choice of mirror radius. The limit is also satisfied by the solutions in Eqs. (18) and (9) for an arbitrary choice of mirror spanning angle θ_m. This result suggests that by utilizing a spherical mirror one can make a tradeoff between measurement imprecision and backaction by choosing an appropriate mirror radius. For a perfectly reflecting hemisphere at $kr_m = n\pi$, the detected scatter is maximally enhanced, but contains no linear position information. Correspondingly, the dominating term of backaction noise vanishes. This reinforces the fact that the flow of energy does not necessarily carry information about the environment with which it has interacted [15,39].

The suppression effect could be tested experimentally by measuring the reheating rates via trapped particle trajectories, as was done in free space [14]. The necessary linear measurement of particle position could be accessed with illumination in the xy plane for a mirror with a spanning angle $\theta_m < \pi/2$, or using a detection beam which does not satisfy the suppression condition for the mirror radius ($kr_m \neq n\pi$). In addition, we note that second-order position information should be accessible under the suppression condition, which is sufficient for the implementation of parametric feedback cooling [40] or temperature measurement.

The largest contributions to residual backaction noise are likely to arise from technical limitations in the experimental realization. According to Eq. (A8), imperfect reflectivity of a metallic mirror affects the suppression result in Eq. (9) linearly, and would limit the suppression of backaction noise to about 10^{-2} of its free-space magnitude. A realization scheme will also require surface quality and long-term mirror radius stability $\delta r_m \ll \lambda/2\pi$. Considering the coefficient of linear expansion of aluminium $\alpha_{\mathrm{Al}} = 2.3 \times 10^{-5}\,\mathrm{K}^{-1}$ and a mirror with radius of about 1 mm, sufficient radius stability can be achieved with thermal stability $\delta T < 1\,\mathrm{K}$. A recent experimental proposal utilizing a spherical mirror for similar application suggests that such temperature stabilization and the quality of the fabricated mirror surface should be achievable [41].

VI. CONCLUSION

In summary, we have found that a suitable structured environment can yield significant reduction of mechanical noise due to backaction. We have studied a spherical mirror as a particular case, and found that it can be used to inhibit the backaction force noise in three dimensions. The suppression scheme also requires the particle to be trapped in a standing-wave trapping field. We have found that under a suitable condition on the mirror radius, the mirror significantly attenuates the attainable acquisition rate of linear position information, at the same time suppressing the largest backaction noise term. In the case that the mechanical noise experienced by the particle is dominated by backaction and the detection is shot-noise limited, we have shown that the imprecision and backaction noise satisfy the Heisenberg limit of detection for any choice of mirror radius r_m and spanning half angle $\theta_m \leqslant \pi/2$. Experimental considerations show that the suppression scheme should be achievable in a realistic setting; the amount by which recoil noise can be suppressed using our method will be limited by either experimental factors (such as mirror reflectivity, thermal stability, or surface quality) or smaller residual backaction noise terms unaccounted for in our calculation.

Counterintuitively, our results show that the suppression condition is also the condition for which the scattered power, usually associated with recoil noise, is maximally enhanced by the spherical mirror. This result suggests that a scheme using a spherical mirror to constrain the backaction noise such as the one analyzed in [26] should aim to maximize scattered radiation instead of suppressing it. Since the scattered power of a particle radiating at the center of a spherical mirror has a sinusoidal dependence on the mirror radius, this change to the protocol of Ref. [26] can be effected with a small adjustment of the mirror radius by $\lambda/4$.

Our result can be understood in the context of the position information content in the outgoing particle scatter; at the suppression condition, the image dipole appears identical to the real particle to first order in particle position about the mirror center, preventing localization in a position tracking experiment. For all experimental conditions considered, we have shown that this measurement imprecision and the corresponding backaction satisfy the Heisenberg limit of detection. The method presented here shows how an appropriate reflective surface geometry can be used to mitigate backaction, and may enable development of more sophisticated schemes for particles of different sizes and shapes in future experiments. In addition, a wider range of geometries may be suitable, if one wishes to suppress the backaction noise only in one or two directions.

The main result shows a strong dependence of the imprecision-backaction characteristics on the surrounding mirror geometry. The spherical mirror geometry is uniquely suited for pointlike particles as the mirror reflection can perfectly match dipole emission away from the mirror. Other geometries may present similar useful properties in future investigations, such as a plane mirror-lens system. Other practical arrangements suitable for the scattering properties of particles with different and more complex morphologies may be found by adapting existing analysis tools, used for tailoring the optical properties of nanoscale emitters [42,43]. We once again note that although the spherical mirror geometry plays a necessary role for the suppression effect, it is not sufficient for full suppression in three dimensions; a standing-wave trapping potential is also required to remove the contribution of the local phase gradient, which would be present in a single-beam configuration [15].

ACKNOWLEDGMENTS

R.G. was supported by the U.K. Engineering and Physical Sciences Research Council through a Standard Research Studentship (Doctoral Training Partnership) Grant No. EP/T517987/1.

DATA AVAILABILITY

No new data were generated or analyzed during this study.

APPENDIX A: SYSTEM'S DYADIC GREEN'S FUNCTION

Green's functions are solutions to inhomogeneous differential equations with the inhomogeneity given by a delta function. In homogeneous space, a point dipole gives a singular inhomogeneity in the Helmholtz equation. Fields radiated by a pointlike electric dipole are determined by the *dyadic Green's function* $\overline{\overline{\mathbf{G}}}$—a tensor of rank 2 which solves the equation [22]

$$\nabla \times \nabla \times \overline{\overline{\mathbf{G}}}(\mathbf{r}, \mathbf{r}_0, \omega) - k^2 \overline{\overline{\mathbf{G}}}(\mathbf{r}, \mathbf{r}_0, \omega) = \overline{\overline{\mathbf{I}}} \delta(\mathbf{r} - \mathbf{r}_0) \quad \text{(A1)}$$

with wave number $k = \omega/c$, unit dyad $\overline{\overline{\mathbf{I}}}$, source position $\mathbf{r}_0$, and observation point $\mathbf{r}$. In free space, the solution for the Green's function is [22]

$$\overline{\overline{\mathbf{G}}}_0(\mathbf{r}, \mathbf{r}_0, \omega) = \left[\overline{\overline{\mathbf{I}}} + \frac{1}{k^2}\nabla\nabla\right] \frac{\exp(ikr')}{4\pi r'} \quad \text{(A2)}$$

where we write $r' = |\mathbf{r}'| = |\mathbf{r} - \mathbf{r}_0|$ and a direct product of two vectors corresponds to a dyadic product. In the subsequent calculations, we will make particular use of the part of $\overline{\overline{\mathbf{G}}}_0$ which scales as $(r')^{-1}$:

$$\overline{\overline{\mathbf{G}}}_{\text{ff}}(\mathbf{r}, \mathbf{r}_0, \omega) = \frac{\exp(ikr')}{4\pi r'} \left[\overline{\overline{\mathbf{I}}} - \frac{\mathbf{r}'\mathbf{r}'}{(r')^2}\right] \quad \text{(A3)}$$

which gives rise to the far-field free-space dipole emission given by

$$\mathbf{E}_s(\mathbf{r}, \mathbf{r}_0) = \frac{k^2}{\epsilon_0} \overline{\overline{\mathbf{G}}}_{\text{ff}}(\mathbf{r}, \mathbf{r}_0, \omega) \cdot \mathbf{p} \quad \text{(A4)}$$

where $\mathbf{p}$ is the electric dipole moment. We can also use the system's dyadic Green's function element corresponding to the dipole orientation to evaluate the correlation functions of the field fluctuations in the framework of stochastic electrodynamics [20,22]. At thermal equilibrium at temperature T this fluctuation-dissipation theorem for the $\hat{\mathbf{x}}$ component of the field fluctuations reads

$$\langle \delta\tilde{E}^*(\mathbf{r}, \omega) \delta\tilde{E}(\mathbf{r}', \omega') \rangle = f(\mathbf{r}, \mathbf{r}'; \omega, T) \delta(\omega - \omega'), \quad \text{(A5)}$$

where

$$f(\mathbf{r}, \mathbf{r}'; \omega, T) = \frac{\hbar\omega^2}{2\pi c^2 \epsilon_0} \coth\left(\frac{\hbar\omega}{2k_B T}\right) \text{Im}[G_{xx}(\mathbf{r}, \mathbf{r}', \omega)]. \quad \text{(A6)}$$

In the main text, we use Eq. (A5) to model the spectral density of force fluctuations due to backaction.

In the presence of reflective boundaries, the total Green's function can be decomposed as

$$\overline{\overline{\mathbf{G}}}(\mathbf{r}, \mathbf{r}_0, \omega) = \overline{\overline{\mathbf{G}}}_0(\mathbf{r}, \mathbf{r}_0, \omega) + \overline{\overline{\mathbf{G}}}_s(\mathbf{r}, \mathbf{r}_0, \omega) \quad \text{(A7)}$$

where the first term corresponds to free-space emission, and the second term corresponds to the *reflected* field and depends on the boundary. For a dipole emitter located at or near the center of a large spherical mirror (with radius $r_m \gg \lambda$), only the far fields contribute to the reflected fields near the source position. Modeling the reflected fields using Fresnel coefficients and the angular spectrum representation for focused far fields [22,30], at an observation point $\mathbf{s}$ at or near the center of the mirror we find the expression

$$\overline{\overline{\mathbf{G}}}_s(\mathbf{s}, \mathbf{r}_0, \omega) = -\rho \frac{ikr_m e^{ikr_m}}{2\pi} \int_{(a)} \overline{\overline{\mathbf{G}}}_{\text{ff}}(\mathbf{r}, \mathbf{r}_0, \omega) e^{-ik\hat{\mathbf{r}}\cdot\mathbf{s}} d\Omega \quad \text{(A8)}$$

where $k = \omega/c$, ρ denotes the Fresnel reflection coefficient of the mirror at normal incidence, $\mathbf{r}$ denotes a vector from the origin to a point on the mirror surface, and the integration of the solid angle element $d\Omega$ runs over the solid angle of the mirror [denoted as domain (a) in Fig. 3].

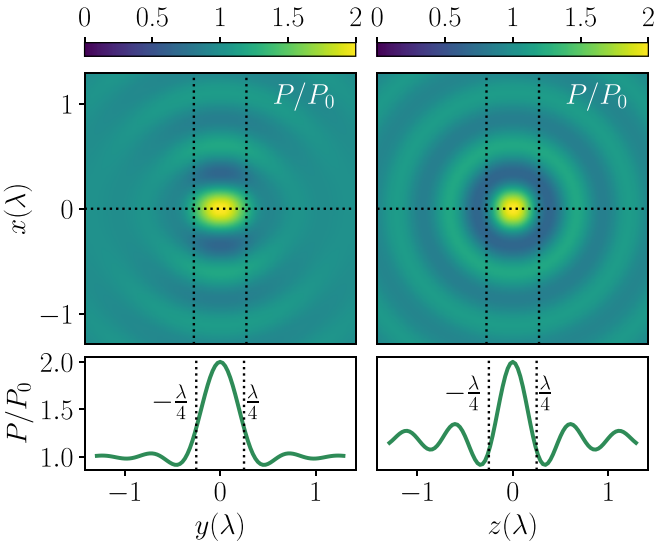

FIG. 5. Modified scattered power, expressed as a ratio with the free-space scattering rate P/P_0, evaluated at the mirror radius condition $kr_m = n\pi$. The modified scattered power for a displaced source is found by numerically solving the scattering Green's function in Eq. (A8).

APPENDIX B: DIPOLE EMISSION NEAR BOUNDARIES

The scattering rate of a point dipole emitter depends on its environment. For a point dipole emitter, the average scattered power can be expressed as [22,43]

$$\langle P \rangle = \frac{6\pi P_0}{k} \mathbf{n}_p \cdot \text{Im}[\overline{\overline{\mathbf{G}}}(\mathbf{r}_0, \mathbf{r}_0, \omega_0)] \cdot \mathbf{n}_p \quad \text{(B1)}$$

where the dyadic Green's function is evaluated at the location of the dipole in both arguments, P_0 denotes he free-space scattered power, and the vector $\mathbf{n}_p$ denotes the dipole orientation. By substituting Eq. (A7) into (B1) and using Eqs. (A2) and (A8), we find that at the center of a perfectly reflecting ($\rho = -1$) hemispherical mirror the scattered power is given by

$$\langle P \rangle = 2\cos^2(kr_m) P_0. \quad \text{(B2)}$$

In agreement with the QED result found for a spontaneous emission from an atom at the center of a hemispherical mirror [23], the condition $kr_m = n\pi$ corresponds to a twofold enhancement of the total scattered power. In Fig. 5 we also

show that the scattered power varies as the location of the dipole is varied about the center of the mirror.

APPENDIX C: RETROREFLECTION FROM A SPHERICAL MIRROR

In this section we find the necessary conditions for retroreflection of a laser beam from the surface of a spherical mirror, and the corresponding mirror radius which allows trapping at the mirror center. The beam is retroreflected when its radius of curvature matches that of the mirror. Modeling the laser as a paraxial Gaussian beam with radius of curvature $R(z)$, this condition is expressed as [44]

$$r_m = R(z - z_f) = z - z_f + \frac{z_R^2}{z - z_f} \tag{C1}$$

where z_f is the axial position of the focus along the mirror axis. The condition in Eq. (C1) has two solutions for the focus position:

$$z_f^{\pm} = \frac{r_m}{2}\left(1 \pm \sqrt{1 - 4\frac{z_R^2}{r_m^2}}\right). \tag{C2}$$

Since we want the laser intensity at the trapping position to be as large as possible, we choose the negative sign solution. Therefore, we can achieve maximum modulation when the beam is focused a distance z_R^2/r_m (for $z_R \ll r_m$) from the mirror center towards its surface. Note that since $z_R \approx \lambda/\pi(\mathrm{NA})^2$ for a beam of numerical aperture NA, the tighter the focus of the beam, the closer the solution z_f^- is to the center of the mirror.

To find a condition on the mirror radius which yields an intensity maximum at the center of the mirror, we consider the round-trip phase about the mirror center. For a plane wave reflecting from a perfect plane mirror a distance r_m away this round-trip phase would simply be equal to $2kr_m + \pi$. For a Gaussian beam, there is an additional contribution arising from the Gouy phase shift $\phi_g(z) = \arctan(z/z_R)$ [37]. With the focus at z_f^- we find that

$$\Delta\phi = 2kr_m + \pi + \underbrace{2[\phi_g(z_f) + \phi_g(r_m - z_f)]}_{\pi} = 2kr_m. \tag{C3}$$

That is, the contribution of the Gouy phase shift to the round-trip phase is equal to exactly π when the beam is retroreflected, such that the total phase is fixed only by the round-trip distance. To ensure that the incident beam is in-phase with its reflection at the center, the mirror radius has to be restricted to $kr_m = n\pi$, for integer n. This condition corresponds to the maximum enhancement of scattered power from a trapped particle. As we discussed in the main text, this condition is exactly the condition needed to achieve suppression of backaction noise acting on a trapped particle. This coincidental feature ensures that the recoil noise suppression condition is matched when the particle is brought to the center of the spherical mirror in a standing wave, formed by reflection from the mirror.

[1] G. Ranjit, M. Cunningham, K. Casey, and A. A. Geraci, Zeptonewton force sensing with nanospheres in an optical lattice, Phys. Rev. A **93**, 053801 (2016).

[2] J. Ahn, Z. Xu, J. Bang, P. Ju, X. Gao, and T. Li, Ultrasensitive torque detection with an optically levitated nanorotor, Nat. Nanotechnol. **15**, 89 (2020).

[3] N. Aggarwal, G. P. Winstone, M. Teo, M. Baryakhtar, S. L. Larson, V. Kalogera, and A. A. Geraci, Searching for new physics with a levitated-sensor-based gravitational-wave detector, Phys. Rev. Lett. **128**, 111101 (2022).

[4] F. Monteiro, G. Afek, D. Carney, G. Krnjaic, J. Wang, and D. C. Moore, Search for composite dark matter with optically levitated sensors, Phys. Rev. Lett. **125**, 181102 (2020).

[5] R. Kaltenbaek *et al.*, Research campaign: Macroscopic quantum resonators (MAQRO), Quantum Sci. Technol. **8**, 014006 (2023).

[6] C. Gonzalez-Ballestero, M. Aspelmeyer, L. Novotny, R. Quidant, and O. Romero-Isart, Levitodynamics: Levitation and control of microscopic objects in vacuum, Science **374**, eabg3027 (2021).

[7] U. Delić, M. Reisenbauer, K. Dare, D. Grass, V. Vuletić, N. Kiesel, and M. Aspelmeyer, Cooling of a levitated nanoparticle to the motional quantum ground state, Science **367**, 892 (2020).

[8] L. Magrini, P. Rosenzweig, C. Bach, A. Deutschmann-Olek, S. G. Hofer, S. Hong, N. Kiesel, A. Kugi, and M. Aspelmeyer, Real-time optimal quantum control of mechanical motion at room temperature, Nature (London) **595**, 373 (2021).

[9] J. Piotrowski, D. Windey, J. Vijayan, C. Gonzalez-Ballestero, A. de los Ríos Sommer, N. Meyer, R. Quidant, O. Romero-Isart, R. Reimann, and L. Novotny, Simultaneous ground-state cooling of two mechanical modes of a levitated nanoparticle, Nat. Phys. **19**, 1009 (2023).

[10] A. Militaru, M. Rossi, F. Tebbenjohanns, O. Romero-Isart, M. Frimmer, and L. Novotny, Ponderomotive squeezing of light by a levitated nanoparticle in free space, Phys. Rev. Lett. **129**, 053602 (2022).

[11] A. B. M. V. B. Braginskĭ, *Measurement of Weak Forces in Physics Experiments* (University of Chicago, Chicago, 1977).

[12] C. M. Caves, Quantum-mechanical radiation-pressure fluctuations in an interferometer, Phys. Rev. Lett. **45**, 75 (1980).

[13] A. A. Clerk, M. H. Devoret, S. M. Girvin, F. Marquardt, and R. J. Schoelkopf, Introduction to quantum noise, measurement, and amplification, Rev. Mod. Phys. **82**, 1155 (2010).

[14] V. Jain, J. Gieseler, C. Moritz, C. Dellago, R. Quidant, and L. Novotny, Direct measurement of photon recoil from a levitated nanoparticle, Phys. Rev. Lett. **116**, 243601 (2016).

[15] F. Tebbenjohanns, M. Frimmer, and L. Novotny, Optimal position detection of a dipolar scatterer in a focused field, Phys. Rev. A **100**, 043821 (2019).

[16] C. Gonzalez-Ballestero, J. A. Zielińska, M. Rossi, A. Militaru, M. Frimmer, L. Novotny, P. Maurer, and O. Romero-Isart, Suppressing recoil heating in levitated optomechanics using squeezed light, PRX Quantum **4**, 030331 (2023).

[17] G. Winstone *et al.* (LSD Collaboration), Optical trapping of high-aspect-ratio NaYF hexagonal prisms for kHz-MHz gravitational wave detectors, Phys. Rev. Lett. **129**, 053604 (2022).

[18] F. Tebbenjohanns, A. Militaru, A. Norrman, F. van der Laan, L. Novotny, and M. Frimmer, Optimal orientation detection of an anisotropic dipolar scatterer, Phys. Rev. A **105**, 053504 (2022).

[19] K. Sinha and Y. Subaşı, Quantum Brownian motion of a particle from Casimir-Polder interactions, Phys. Rev. A **101**, 032507 (2020).

[20] L. Novotny, M. Frimmer, A. Militaru, A. Norrman, O. Romero-Isart, and P. Maurer, Optomechanical sideband asymmetry explained by stochastic electrodynamics, Phys. Rev. A **106**, 043511 (2022).

[21] G. S. Agarwal, Quantum electrodynamics in the presence of dielectrics and conductors. I. Electromagnetic-field response functions and black-body fluctuations in finite geometries, Phys. Rev. A **11**, 230 (1975).

[22] L. Novotny and B. Hecht, *Principles of Nano-Optics* (Cambridge University Press, New York, 2012).

[23] G. Hétet, L. Slodička, A. Glätzle, M. Hennrich, and R. Blatt, QED with a spherical mirror, Phys. Rev. A **82**, 063812 (2010).

[24] G. Cerchiari, L. Dania, D. S. Bykov, R. Blatt, and T. E. Northup, Position measurement of a dipolar scatterer via self-homodyne detection, Phys. Rev. A **104**, 053523 (2021).

[25] L. Dania, K. Heidegger, D. S. Bykov, G. Cerchiari, G. Araneda, and T. E. Northup, Position measurement of a levitated nanoparticle via interference with its mirror image, Phys. Rev. Lett. **129**, 013601 (2022).

[26] Y. Weiser, T. Faorlin, L. Panzl, T. Lafenthaler, L. Dania, D. S. Bykov, T. Monz, R. Blatt, and G. Cerchiari, Back action suppression for levitated dipolar scatterers, Phys. Rev. A **111**, 013503 (2025).

[27] J. R. Zurita-Sánchez, J.-J. Greffet, and L. Novotny, Friction forces arising from fluctuating thermal fields, Phys. Rev. A **69**, 022902 (2004).

[28] C. Henkel, K. Joulain, J.-P. Mulet, and J.-J. Greffet, Radiation forces on small particles in thermal near fields, J. Opt. A: Pure Appl. Opt. **4**, S109 (2002).

[29] T. Agrenius, C. Gonzalez-Ballestero, P. Maurer, and O. Romero-Isart, Interaction between an optically levitated nanoparticle and its thermal image: Internal thermometry via displacement sensing, Phys. Rev. Lett. **130**, 093601 (2023).

[30] L. Mandel and E. Wolf, *Optical Coherence and Quantum Optics* (Cambridge University Press, New York, 1995).

[31] See Supplemental Material at http://link.aps.org/supplemental/10.1103/PhysRevResearch.7.023041 for more details derivation in Sec. 2, where we also recover the freespace backaction expressions.

[32] T. Seberson and F. Robicheaux, Distribution of laser shot-noise energy delivered to a levitated nanoparticle, Phys. Rev. A **102**, 033505 (2020).

[33] S. Y. Buhmann and D.-G. Welsch, Dispersion forces in macroscopic quantum electrodynamics, Prog. Quantum Electron. **31**, 51 (2007).

[34] L. Martinetz, K. Hornberger, and B. A. Stickler, Surface-induced decoherence and heating of charged particles, PRX Quantum **3**, 030327 (2022).

[35] J. Hüpfl, F. Russo, L. M. Rachbauer, D. Bouchet, J. Lu, U. Kuhl, and S. Rotter, Continuity equation for the flow of Fisher information in wave scattering, Nat. Phys. **20**, 1294 (2024).

[36] See Supplemental Material at http://link.aps.org/supplemental/10.1103/PhysRevResearch.7.023041 for a detailed derivation in Sec. 1.

[37] S. Feng and H. G. Winful, Physical origin of the Gouy phase shift, Opt. Lett. **26**, 485 (2001).

[38] The image of a point scatterer at $\mathbf{r}_0$ near the center of a spherical mirror appears at the reflected position $-\mathbf{r}_0$, for $|\mathbf{r}_0| \ll \lambda$.

[39] J. Hüpfl, F. Russo, L. M. Rachbauer, D. Bouchet, J. Lu, U. Kuhl, and S. Rotter, A continuity equation for the flow of Fisher information in electromagnetic scattering, in *CLEO 2023* (Optica, New York, 2023), p. FW4D.4.

[40] J. Gieseler, B. Deutsch, R. Quidant, and L. Novotny, Subkelvin parametric feedback cooling of a laser-trapped nanoparticle, Phys. Rev. Lett. **109**, 103603 (2012).

[41] G. Araneda, G. Cerchiari, D. B. Higginbottom, P. C. Holz, K. Lakhmanskiy, P. Obšil, Y. Colombe, and R. Blatt, The Panopticon device: An integrated Paul-trap–hemispherical mirror system for quantum optics, Rev. Sci. Instrum. **91**, 113201 (2020).

[42] S. Mignuzzi, S. Vezzoli, S. A. R. Horsley, W. L. Barnes, S. A. Maier, and R. Sapienza, Nanoscale design of the local density of optical states, Nano Lett. **19**, 1613 (2019).

[43] W. L. Barnes, S. A. R. Horsley, and W. L. Vos, Classical antennas, quantum emitters, and densities of optical states, J. Opt. **22**, 073501 (2020).

[44] C. C. Davis, The optics of Gaussian beams, in *Lasers and Electro-Optics: Fundamentals and Engineering*, 2nd ed. (Cambridge University Press, New York, 2014), pp. 438–480.